Journal of Low Temperature Physics
https://doi.org/10.1007/s10909-023-03001-0

Enhanced Delivery and Detection of Terahertz Frequency Radiation from a Quantum Cascade Laser Within Dilution Refrigerator

M. Vaughan[1] · W. Michailow[2] · M. Tan[2] · M. Salih[1] · L. Li[1] · H. Beere[2] · D. A. Ritchie[2] · E. H. Linfield[1] · A. G. Davies[1] · J. E. Cunningham[1]

Received: 5 June 2023 / Accepted: 10 September 2023

Abstract
We report on significant enhancements to the integration of terahertz (THz) quantum cascade lasers (QCL) and THz detection with a two-dimensional electron gas (2DEG) within a dilution refrigerator obtained by the inclusion of a multi-mesh 6 THz low-pass filter to block IR radiation, a Winston cone to focus light output, and gating the 2DEG for optimised sensitivity. We show that these improvements allow us to obtain a >2.5 times reduced sample electron temperature (160 mK compared with 430 mK previously), during cyclotron resonance (CR) measurements of a 2DEG under QCL illumination. This opens up a route to performing sub-100 mK experiments using excitation by THz QCLs.

Keywords Condensed matter · Terahertz · Quantum cascade laser · 2-Dimensional electron gas · milli-Kelvin · Waveguide

1 Introduction

Condensed matter systems (including topological materials, antiferromagnets, and semiconductor mesoscopic systems) often have energy scales commensurate with terahertz (THz) photon energies, or intrinsic timescales in the picosecond range, commensurate with a THz cycle time. Many of these states and transitions are either easier to study or can only be observed at very low (<4 K) temperatures [1–5].

✉ M. Vaughan
eenmv@leeds.ac.uk; M.T.Vaughan@leeds.ac.uk

J. E. Cunningham
J.E.Cunningham@leeds.ac.uk

[1] School of Electronic and Electrical Engineering, University of Leeds, Leeds LS2 9JT, West Yorkshire, UK

[2] Cavendish Laboratory, University of Cambridge, Cambridge CB3 0HE, UK

Published online: 05 October 2023

THz frequency quantum cascade lasers (QCLs) are an established source of high power (mW to W) range THz radiation [6–8], and as such offer great potential for the excitation of condensed matter systems. Unfortunately, THz QCLs currently require cryogenic cooling for optimal performance and have limited wall-plug efficiency, thus presenting a high thermal load on low-temperature cryostats, which is a problem owing to the limited cooling power available at the lowest temperatures (typically only < 1000 μW 100 mK). Recently, we presented a potential solution [9] by showing that THz QCLs could be thermally anchored to one of the higher temperature stages within a pulse tube cooled dilution refrigerator, with a suitable copper THz waveguide used to collect and transmit the THz radiation emitted from the QCL into the sample space.

In our previous work we successfully introduced THz radiation into the sample space of a dilution refrigerator using 6.4 mm-diameter hollow metal waveguides (HMWG). The HMWG collected radiation from a THz QCL located on the first stage pulse tube (held at ~ 48 K with ~ 40 W of cooling power) before transmitting this radiation to the sample space with a total loss of − 9 dB and upwards of 2.8mW of peak power (which had 250 μW of cooling power at 100 mK) [9]. We previously estimated that the sample space to MC chamber thermal resistance was 1.87 $\mathrm{mK\mu W^{-1}}$, so that an increase from the unmodified fridge of 99–206 mK would be caused by ~ 60 μW of heating, which is a significant amount of heating for a sample in a dilution refrigerator.

Our focus previously was on limiting heat conduction through the HMWG walls, achieved using novel thermal isolators between sections of waveguide, while making no attempt to limit blackbody radiation along the waveguides from the pulse tube stage. However, it is important to consider such blackbody radiation, for example, if we approximate using Stefan-Boltzmann's law ($P_{ower}=A_{rea}\varepsilon_{emissvity}\sigma_{const.}T_{emp.}{}^{4}$), that the 4.6 mm waveguide opening ($A_{rea}=16.6$ mm^2) as an ideal blackbody ($\varepsilon_{emissvity}=1$) at $T_{emp.}=290$ K (the temperature of the outer cryostat walls). Then we can estimate that up to $P_{ower}=6$ mW of 290 K blackbody radiation enters the HMWG.

In addition to the higher base temperature induced by the thermal loading from blackbody radiation coupled down the waveguide, power from the THz radiation introduced into the sample space can also degrade the base temperature. We previously found by in-situ sample thermometry that the lowest temperature we could obtain was 430 mK in an exemplar experiment measuring cyclotron resonance (CR) induced by the QCL in a two-dimensional electron gas (2DEG).

However, the active area of the hall bar structure sample was 80 μm by 720 μm (Area = 0.06 mm^2) which is small compared with the area of the 4.6 mm HMWG (16.6 mm^2), such that the majority of the THz power leaving the waveguide was dissipated unnecessarily into the sample space. It would be trivial to increase the size of the active region to capture more THz, but for some condensed matter systems this is not feasible such as quantum dots and microscale antennas [4, 10]. Increasing power density in these cases is preferred.

In our previous work we used an ungated 2DEG as a sample and looked at the CR response as an exemplar physical effect to study. We expect a maximum response when the CR point lies within a quantum Hall effect (QHE) plateau, and a minimum

when between plateaux. This is because the Shubnikov–de Haas (SdH) amplitude is largest between Hall plateaux, which can obscure the CR signal. To maximise the sensitivity of the 2DEG we need to modify the carrier concentration in order to shift the position of the SdH peaks away from the expected CR point. This is most easily achieved by gating the device.

We show here that with better focusing of THz radiation onto the sample active region and matching of the cross-sectional output of the waveguide to the sample area, together with a gate-tuning approach to positioning the transitions between Landau levels in the sample, allows us to obtain the same measurement signal-to-noise ratio for far lower incident THz powers.

In summary, to achieve lower sample temperatures, we sought: (1) better isolation from blackbody radiation transmitted from the higher temperature stages in the refrigerator, and; (2) better spatial matching between the waveguide output and the sample.

2 Setup and Enhancements

As in our previous work a 2.68 THz QCL exploiting a bound-to-continuum [11] design with a power of 22 mW was fitted into a dry dilution refrigerator (Oxford Instruments DR200) (Fig. 1a) on the PT1 plate, with the QCL-THz radiation collected and directed by HMWG into the sample space. The QCL mounting block also securely holds the large 4.6 mm HMWG opening making alignment by eye trivial. The PT1 stage has 40 W of cooling power at 48 K, the waste heat generated by the QCL is kept below 2 W as to not advisedly affect the normal operation of lower cooling stages. HYSOL thermal isolators (Fig. 1b) and compression fittings (Fig. 1c) were used as thermal breaks and mechanical support, respectively.

The sample space was positioned in the bore of a 12 T superconducting solenoid magnet. As a consequence there are a long set of copper rods (256 mm) connecting the sample space to the mixing chamber plate which introduces some thermal resistance between the final cooling stage and the sample. The mixing chamber is typically at 33mK as compared to the sample which is at 99mK for our original unmodified fridge. As such, preventing heat leaking into the sample space is important given the already large difference in temperature between the two stages.

2.1 QMC Low Pass Filter

To reduce the heating we need a way to prevent warm 290 K radiation from the cryostat inner walls propagating along the HMWG. Limited space, QCL power wires, alignment and ease of access make covering the entire QCL fixture difficult. Instead a multi-mesh filter was included utilising a capacitive grid array geometry, with a low-pass cut-off at 6 THz [12, 13], located inside a compression fitting on the PT2 plate (Fig. 1c). In addition, a Winston cone with a 1 mm-diameter aperture positioned as close as possible to the sample (Fig. 1d). The PT2 plate was chosen as it is the coldest stage (3.5 K) that still has significant cooler power (4 W) sufficient to

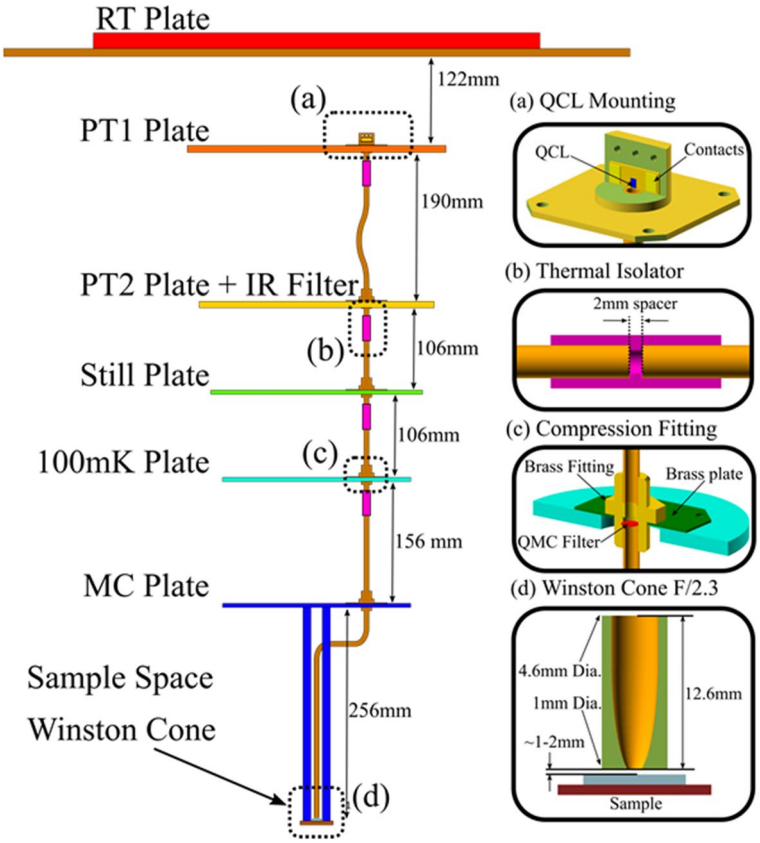

Fig. 1 Waveguide system inside the refrigerator with **a** the THz QCL, **b** thermal isolators, and **c** compression fittings. A 6 THz low pass filter was located inside the compression fitting on the PT2 plate. **d** A Winston cone was positioned as close as possible to the sample to maximize coupling. RT plate is room temperature, PT1/2 are the pulse to first and second stages respectively and MC plate is the mixing chamber

cool the QMC filter. The transmission spectrum of the multi-mesh filter is shown in Fig. 2, along with a 290 K blackbody spectrum before and after filtering. The filter transmits ~ 80% of our QCL radiation at 2.6 THz, while blocking 97% of the incident blackbody radiation.

The QMC filter was placed inside the compression fitting on the PT2 plate. Extra space (~ 1 mm) is added to each compression fitting allowing for thermal contraction, which is sufficient space to accommodate the 100 μm-thick filters. The filter will also block ~ 50% of the blackbody radiation from the PT1 plate at 50 K, although at 50 K source produces 1130 times less radiative power than a 290 K source.

With the inclusion of the multi-mesh filter to block blackbody radiation leaking into the coldest stages we improved the base temperature from our previous lowest of 209 mK, to 114 mK, which was only 25 mK higher than the base temperature of

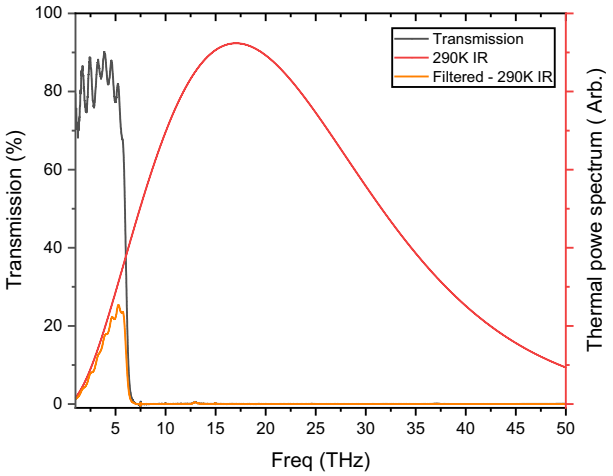

Fig. 2 (Black) 6 THz low-pass filter (QMC Instruments) transmission spectrum. (Red) 290 K ideal blackbody spectrum, from Planck's Law. (Orange) blackbody radiation after filtering. The QMC filter blocks an estimated ~ 97% of IR radiation [12]

99 mK obtained before introduction of the waveguides, implying that roughly ~ 80% of the heat leaking to the sample space was blackbody radiation from the room temperature cryostat walls at 290 K. We attribute the remainder as likely to arise from small residual heat leaks between our thermal HYSOL isolators.

2.2 Winston Cone

To increase the power density at the active region of the sample we need a method of focusing THz radiation. Several methods exist for focusing including lenses and exploiting a self-focusing effect beyond straight sections of HMWG [14]. We chose to place a Winston Cone with an entrance aperture of diameter 4.6 mm (the same as the HMWG inner diameter), and an exit aperture of diameter 1 mm (0.8 mm^2 area), immediately above the sample (Fig. 1d), increasing the power density by around 21 times. For the measurements reported here, the sample active region had an area of 0.06 mm^2, to allow for some degree of misalignment. The Winston Cone was registered to the center of the sample position using a copper bracket, and was vertically adjusted to be as close as possible to the sample (approximately 1–2 mm) without risking contact with, or shorting of, the sample bond wires.

2.3 Gated 2-Dimension Electron Gas

Our previous THz detector relied on a 2DEG where the CR response occurs at the same B field as a peak in resistance from the SdH, reducing the sensitivity of the device. We then looked to use a 2DEG with an added top gate which would allow us

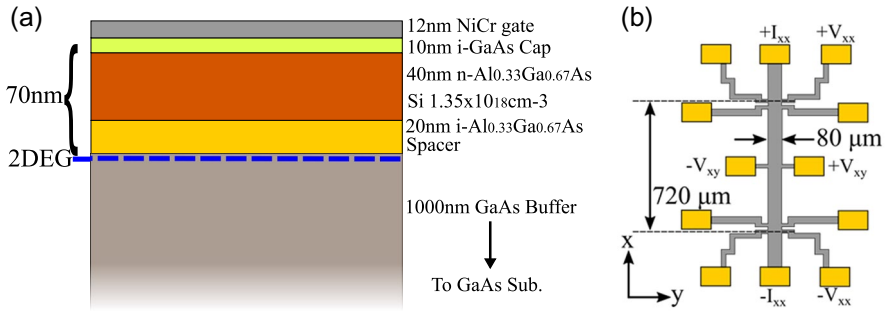

Fig. 3 **a** Layer structure of the AlGaAs/GaAs 2DEG grown on a GaAs substrate. A 12 nm-thick NiCr gate deposited on the top surface of the device was used to modify the carrier concentration. **b** Hall bar pattern with the 6 point electrical measurement layout, NiCr gate covers whole device (not shown)

to modify the carrier concentration and SdH oscillation peak positions to be tuned to maximise the signal-to-noise ratio.

By using a top gated AlGaAs/GaAs 2DEG to detect the THz, the position of the SdH resistance peaks of our sample could be optimised for detection by tuning the gate bias for our specific incident QCL frequency (Fig. 3a). The gate was an 11.7 ± 0.5 nm layer of NiCr, a thickness chosen to be continuous but still reasonably transparent. While we calculate that the gate only transmits 30%, absorbs 20% and reflects the remaining THz radiation [15], the increase in sensitivity resulting from being able to tune the carrier concentration was nonetheless significant in allowing us to achieve the observed lower sample temperatures.

The low-pass filter, the Winston cone and the use of a gated 2DEG thus had the effect of reducing heat leaks, increasing power density and increasing sensitivity respectively.

3 Results

In measurements of our 2DEG, the position of the CR can be estimated by measuring the effective mass since we know (from independent Fourier-transform infrared spectroscopy measurements) the QCL frequency. The electric transport was measured in a Hall bar geometry with 6 points of electrical constant by applying 100 nA AC current at 127 Hz, while using 2 lock-in amplifiers to measure the longitudinal (R_{xx}) and transverse (R_{xy}) voltages (Fig. 3b), results of which are shown in Fig. 4.

$$\Delta R = 4R_0 e^{-\beta T_D} \frac{\beta T}{\sinh \beta T} \; where \; \beta = \frac{2\pi^2 K_B m_*}{\hbar e B}, \tag{1}$$

The effective mass was measured using a series of temperature and magnetic field sweeps and then employing the Lifshitz–Kosevich (LK) equation (Eq. 1) [16]. Here ΔR is the change in resistance, R_0 is the $B=0$ resistance, T is temperature, T_D

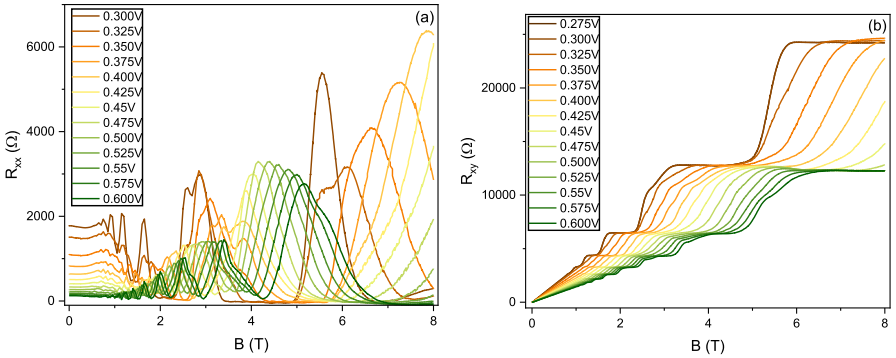

Fig. 4 R_{xx} and R_{xy} of the 2DEG at varying gate bias from 0.3 to 0.6 V. By modifying the carrier concentration the position of the Hall plateaus and the SdH peak positions can be moved with respect to the fixed CR point, thus optimising the detection of THz radiation from the QCL

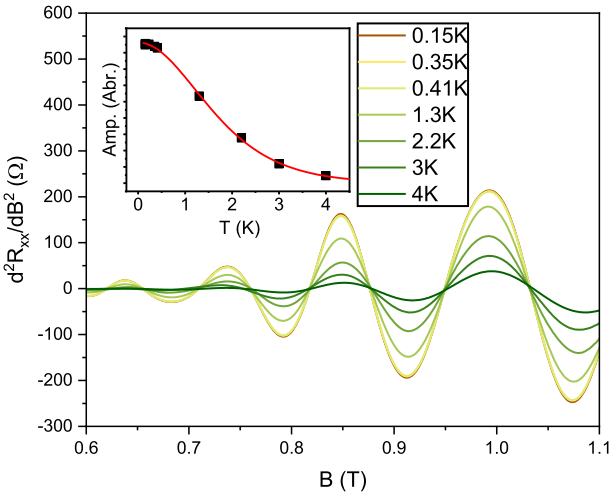

Fig. 5 The second derivative of the longitudinal resistance (R_{xx}) with respect to B at increasing temperatures. (Insert) SdH oscillation amplitudes (at 0.84 T) are plotted against temperature. Using LK equation (Eq. 1) we obtained an effective mass of 0.073 ± 0.001 m_e

is the Dingle temperature, m_* is the effective mass, and the rest are physical constants (K_B, $\hbar$ and e). This gave an effective mass of 0.073 ± 0.001 m_e. We can estimate the position of the CR peak using the cyclotron resonance frequency equation $B = 2\pi f m_*/e$, by combining the known QCL frequency of $f = 2.68$ THz and the effective mass (m_*), we expect to obtain a CR response at $B = \sim 6.94$ T (Fig. 5).

To maximize the THz photovoltage we switched the 127 Hz AC 100nA source to a DC 100nA source and used a reference signal from the QCL pulse modulation (10% duty cycle at 950 mA) also at a frequency of 127 Hz for the lock-in amplifiers. This method is most sensitive to the THz-induced photovoltage of the sample and less sensitive to any (much slower) thermal response or other noise sources. We

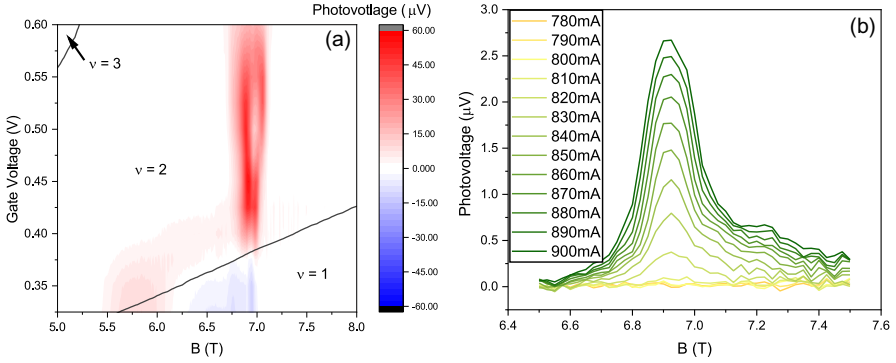

Fig. 6 **a** 2D plot of the CR photovoltage at 950 mA and 10% duty cycle QCL power versus gate bias and magnetic field, measured using a constant 100 nA DC current while locking-in to the QCL pulse frequency. Contour lines show the boundary between QHE plateaus, each labelled with a corresponding filling factor (ν). **b** Low QCL current sweeps of the CR response, with the lowest observable CR response found at 820 mA. Gate bias was set at 0.36 V

investigated the full magnetic field response of the CR versus gate bias (Fig. 6a). The sample response was found to be strongly dependant on gate bias and largest near the expected CR position. Contour lines in Fig. 6a show the rough boundary between filling factors and as expected the 2DEG has the greatest sensitivity when the peaks in the SdH response are positioned away from the expected CR point for our QCL frequency. The main CR peak was measured to occur at ~ 6.93 T, which is similar to the expected value we estimate from the effective mass (~ 6.94 T).

Curiously, we note there are multiple peaks in the 2D map of CR response. We can assume that the QCL frequency is unaffected by sample gate bias or the weak stray field (< 10 mT). Much larger magnetic fields, > 1 T, can cause Landau splitting in QCL structures and shift the position of the central frequency [17]. The cause of the multiple peaks may be small differences in effective mass. Assuming a fixed QCL frequency our effective mass would need to range from 0.072 to 0.074 m_e.

When accounting for hysteresis in the gate (by sweeping the gate bias starting at 0 V) we obtained the largest photovoltage, and so maximum sensitivity, at 6.93 T and for a gate bias of 0.36 V. At this point (0.36 V) the carrier concentration was found to be ~ 2.73×10^{11} cm^{-2} while the mobility was 2.85×10^5 cm^2V^{-1} s^{-1}. Sweeping field while progressively incrementing the QCL power to lower values, we found that the lowest QCL power for which a CR was unambiguously seen corresponded to a QCL excitation current of 820 mA (Fig. 6b).

With the QCL at 900 mA we estimate that ~ 30 μW of THz illumination was arriving at the sample space, Taking into account the aperture of the Winston cone opening, and the active region of the device, the 2.67 μV maximum response for the sample provides an estimate of sensitivity as a 0.09 VW^{-1}, or 2 $mVmicroW^{-1}cm^2$ for our detection of the Terahertz radiation.

We then needed to ascertain the sample temperature under these conditions. For this we require some property of the sample that is strongly dependent on temperature at milli-Kelvin temperatures in order to calibrate the effect and use it as a direct

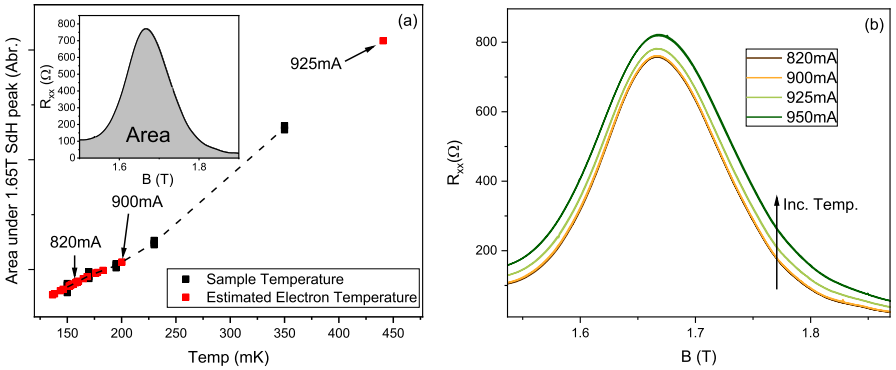

Fig. 7 **a** The sample electron temperature is estimated from calibrating the area under the 1.65 T R_{xx} peak (see insert) at various sample space temperatures. **b** The same section of R_{xx} at base temperature under THz illumination, for high QCL (> 900 mA) currents there is a clear increase in the overall resistance. The minimum detectable photovoltage (obtained at a QCL current of 820 mA, see Fig. 6b) produced an electron temperature of ~ 160 mK

local thermometer. This is because the normal sample space thermometer has insufficient thermal contact for a source of heating directly on the sample.

Peaks in the SdH response for an electron gas [18] are well known to change their shape with temperature; since the electron thermalization timescale is very short (femto-seconds) they are a good proxy for the bulk sample temperature [19]. We chose to measure the area under the 1.65 T peak (Fig. 7 inset) since it showed a strong relationship with temperature, ideal for generating a calibration curve. The area under the peak was measured at increasing known sample space temperatures from which a calibration curve can be generated(black line/points Fig. 7a) we can then estimate the sample electron temperature while undergoing THz illumination.

We then applied THz radiation to the device and estimated the sample temperature (Fig. 7a red points and Fig. 7b). At the lowest QCL power for which a CR response is seen, at 820 mA (Fig. 6a), the estimated sample temperature was ~ 160 mK. This is a substantial improvement over the 430 mK achieved in our previous work. From Fig. 7 we can also see that there is still sufficient power in the QCL THz radiation to significantly heat the sample space despite any extra losses in the HMWG assembly from the QMC filter and Winston cone.

4 Conclusions

We have demonstrated significant enhancement to the lowest temperature experiments yet undertaken using an in-situ THz QCL for signal excitation in a dilution refrigerator, obtaining a 160 mK sample electron temperature while still observing a THz response. This was achieved by the introduction of a low-pass 6 THz filter, a Winston cone and an optimised detection with a gated 2DEG sample, with these modifications improving isolation from the environment, increasing the power density of the THz illumination and enhancing sensitivity to THz radiation, respectively.

We note that alternative geometries for mounting the QCL would be possible, including the use of free-space optics to couple radiation from the QCL to the sample space, though this arrangement could be difficult to align given the likely contraction of larger optical elements during cooling from room temperature.

Further improvements would likely require a dilution fridge with a higher cooling power to counteract heating from the THz illumination from the QCL itself, as well as reduction of the small residual heat leaks between waveguide sections. Optimizing the detection of THz radiation with a 2DEG could also be improved by using a back gate instead of a lossy top gate and larger active region. It appears likely that sub-100 mK experiments using the radiation from THz QCLs could be reached using a combination of such developments.

Acknowledgements The authors acknowledge EPSRC funding (Grants EP/P021859/1, EP/W028921/1, and EP/V004743/1). W.M. thanks Trinity College Cambridge for a Junior Research Fellowship. Thanks also goes to Yuqing Wu for helping with device fabrication.

Author contributions M. Vaughan and J. E. Cunningham wrote the amin manuscript. W. Michailow, M. Tan, H. Beere, D. A. Ritchie provided samples and supporting data for samples. M. Salih, L. Li, E. H. Linfield, A. G. Davies provide the quantum cascade laser source and supporting data. All authors reviewed the manuscript.

Data Availability Data for this work is openly available and stored by the University of Leeds data repository [20].

Declarations

Competing interests The authors declare no competing interests.

References

1. H. Plank et al., Infrared/terahertz spectra of the photogalvanic effect in (Bi, Sb)Te based three-dimensional topological insulators. Phys. Rev. Mater. **2**(2), 024202 (2018). https://doi.org/10.1103/PhysRevMaterials.2.024202
2. R. Khymyn, I. Lisenkov, V. Tiberkevich, B.A. Ivanov, A. Slavin, Antiferromagnetic THz-frequency Josephson-like oscillator driven by spin current. Sci. Rep. **7**(1), 1–10 (2017). https://doi.org/10.1038/srep43705
3. W. Du, Y. Huang, Y. Zhou, X. Xu, Terahertz interface physics: from terahertz wave propagation to terahertz wave generation. J. Phys. D Appl. Phys. **55**(22), 223002 (2022). https://doi.org/10.1088/1361-6463/ac3f58
4. Y. Kawano, Terahertz waves: a tool for condensed matter, the life sciences and astronomy. Contemp. Phys. **54**(3), 143–165 (2013). https://doi.org/10.1080/00107514.2013.817194

5. F. Gouider et al., Magnetotransport and THz-optical investigations at devices with HgTe quantum wells. J. Low Temp. Phys. **159**(1–2), 184–188 (2010). https://doi.org/10.1007/s10909-009-0115-5
6. A. Leitenstorfer et al., The 2023 terahertz science and technology roadmap. J. Phys D **56**, 223001 (2023). https://doi.org/10.1088/1361-6463/acbe4c
7. R. Köhler et al., Terahertz semiconductor-heterostructure laser. Nature **417**(6885), 156–159 (2002). https://doi.org/10.1038/417156a
8. L.H. Li et al., Multi-Watt high-power THz frequency quantum cascade lasers. Electron. Lett. **53**(12), 799–800 (2017). https://doi.org/10.1049/el.2017.0662
9. M. Vaughan et al., Directed delivery of terahertz frequency radiation from quantum cascade lasers within a dry 3He dilution refrigerator. Rev. Sci. Instrum. **93**(11), 113906 (2022). https://doi.org/10.1063/5.0102553
10. W. Michailow et al., An in-plane photoelectric effect in two-dimensional electron systems for terahertz detection. Sci. Adv. **8**(15), 1–18 (2022). https://doi.org/10.1126/sciadv.abi8398
11. G. Scalari et al., Far-infrared ($\lambda \simeq 87$ μm) bound-to-continuum quantum-cascade lasers operating up to 90 K. Appl. Phys. Lett. **82**(19), 3165–3167 (2003). https://doi.org/10.1063/1.1571653
12. QMC Instruments, Multi-mesh filters, www.qmcinstruments.co.uk/multi-mesh-filters
13. P.A.R. Ade, G. Pisano, C. Tucker, S. Weaver, A review of metal mesh filters. Millim. Submillim. Detect. Instrum. Astron. III **6275**, 62750U (2006). https://doi.org/10.1117/12.673162
14. W. Michailow, N.W. Almond, H.E. Beere, D.A. Ritchie, Cylindrical multimode waveguides as focusing interferometric systems. ACS Photonics (2022). https://doi.org/10.1021/acsphotonics.2c02030
15. D.X. Zhou, E.P.J. Parrott, D.J. Paul, J.A. Zeitler, Determination of complex refractive index of thin metal films from terahertz time-domain spectroscopy. J. Appl. Phys. **104**(5), 53110 (2008). https://doi.org/10.1063/1.2970161
16. D. Shoenberg, *Magnetic Oscillations in Metals* (Cambridge University Press, 1984). https://doi.org/10.1017/cbo9780511897870
17. V. Tamosiunas et al., Terahertz quantum cascade lasers in a magnetic field. Appl. Phys. Lett. **83**(19), 3873–3875 (2003). https://doi.org/10.1063/1.1626018
18. K. Saeed et al., Impact of disorder on frequency scaling in the integer quantum Hall effect. Phys. Rev. B Condens. Matter Mater. Phys. **84**(15), 155324 (2011). https://doi.org/10.1103/PhysRevB.84.155324
19. X. Zhao, B. Nabet, Monte Carlo simulation of transport in two-dimensional electron gas via energy relaxation, in *2005 NSTI Nanotechnology Conference and Trade Show—NSTI Nanotech 2005 Technical Proceedings* (2005), pp. 84–86.
20. M. Vaughan, W. Michailow, M. Tan, M. Salih, L. Li, H. Beere, D.A. Ritchie, E.H. Linfield, A.G. Davies, J.E. Cunningham, Dataset associated with 'Enhanced delivery of terahertz frequency radiation from a quantum cascade laser within a dry 3He dilution refrigerator' (2023). https://doi.org/10.5518/1381